Sains Malaysiana 40(6)(2011): 631–636

Comparison of Mesa and Device Diameter Variation in Double Wafer-Fused Multi Quantum-Well, Long-Wavelength, Vertical Cavity Surface Emitting Lasers

(Perbandingan Variasi Diameter Peranti dan Mesa dalam Laser Pemancar Permukaan dengan Rongga Menegak dan Perigi Kuantum Berbilang yang Dilakur Wafer Secara Berganda)

P. S. MENON*, K. KANDIAH, B. Y. MAJLIS & S. SHAARI

ABSTRACT

Long-wavelength vertical-cavity surface-emitting lasers (LW-VCSELs) have profound advantages compared to traditional edge-emitting lasers offering improved properties with respect to mode selectivity, fibre coupling, threshold currents and integration into 2D arrays or with other electronic devices. Its commercialization is gaining momentum as the local and access network in optical communication system expand. Numerical modeling of LW-VCSEL utilizing wafer-fused InP-based multi-quantum wells (MQW) and GaAs-based distributed Bragg reflectors (DBRs) is presented in this paper. Emphasis is on the device and mesa/pillar diameter design parameter comparison and its effect on the device characteristics.

Keywords: GaAs; InP; mesa; multi quantum well; semiconductor laser

ABSTRAK

Laser pemancar permukaan dengan rongga menegak untuk jarak gelombang panjang (LW-VCSEL) mempunyai kelebihan yang lebih nyata berbanding laser pemancar sisi konvensional. Kelebihannya termasuklah kebolehan melakukan pemilihan mod, gandingan gentian, arus ambang yang rendah dan pengintegrasian ke dalam jujukan 2D atau sebarang peranti elektronik lain. Momentum pengkomersialannya semakin meningkat di dalam rangkaian tempatan dan capaian apabila sistem komunikasi optik semakin berkembang. Pemodelan berangka LW-VCSEL yang menggunakan perigi kuantum berbilang (MQW) berasaskan substrat InP yang terlakur wafer dan pemantul Bragg teragih (DBR) yang berasaskan substrat GaAs dipersembahkan di dalam kertas ini. Penekanan diberikan terhadap perbandingan parameter reka bentuk diameter dan mesa dan kesannya terhadap pelbagai pencirian peranti.

Kata kunci: GaAs; InP; laser semikonduktor; mesa; perigi kuantum berbilang

INTRODUCTION

Long wavelength VCSELs at 1.3 and 1.55 μm provide the advantage of having higher bit rates over longer distances while maintaining the cost factor and this is crucial especially in access and backbone optical communication networks (Kapon & Sirbu 2009). VCSELs operating in the 1.55 μm wavelength region have been fabricated using various fabrication techniques such as wafer fusion (Karim et al. 2001; Ohiso et al. 2002; Syrbu et al. 1998), all epitaxial growth (Lin et al. 2003; Nakagawa et al. 2001; Shin et al. 2002; Yuen et al. 2000) and a combination of epitaxially-grown and dielectric distributed Bragg reflectors (DBRs) (Nishiyama et al. 2003; Shau et al. 2001).

In the past, some VCSEL devices developed using the wafer fusion method have achieved continuous wave (CW) operation above 100°C at 1.55 μm at a threshold current and voltage of 1 mA and 2.4V respectively (Karim et al. 2001). Various other researchers have also employed the wafer-fusion method to take advantage of the high gain InP-based active region and high quality GaAs/AlGaAs DBRs (Geske et al. 2004; Margalit et al. 1997; Mehta et al. 2006). Long-wavelength (LW) VCSELs normally employ either InGaAsP, InGaAlAs or AlInGaAs as the active region in the multi quantum well (MQW) layer (Hofmann & Amann 2008; Karim et al. 2001; Mehta et al. 2006).

Reduction in the LW-VCSEL's diameter (active region diameter) increases both the carrier and photon density rates and subsequently reduces the current/gain threshold. The purpose of the air-post design (with a mesa/pillar) is a form of current confinement to inject carriers from the p+-doped region towards the active region and then towards the n+-doped region at the bottom. It also serves to prevent current spreading before the recombination region thus decreasing leakage currents. In this paper, we evaluated the effects of device and mesa diameters on the characteristics of an etched air-post 1.5 μm GaAs/InP-based, double-fused LW-VCSEL using commercial, numerically-based simulation software (SILVACO 2007). The results of this paper provides insight to device designer to determine the best parameter value combination of both the device diameter (L_{DD}) and the mesa or pillar diameter (L_{PD}) to obtain the most optimum device characteristics.

THEORY

The basis of the simulation is to solve two-dimensional Poisson's equation and the continuity equations for electrons and holes. Poisson's equation which is given by (SILVACO 2007):

$$\nabla \bullet (\in \nabla \Psi) = \rho \tag{1}$$

relates variations in electrostatic potential ψ to local charge densities ρ and the local permittivity ε. The continuity equations are given by (SILVACO 2007):

$$\frac{\partial n}{\partial t} = G_n - R_n + \frac{1}{q}\nabla.\vec{J}_n \tag{2}$$

$$\frac{\partial p}{\partial t} = G_p - R_p + \frac{1}{q}\nabla.\vec{J}_p \tag{3}$$

where n and p are the electron and hole concentrations, J_n and J_p are the electron and hole current densities, G_n and G_p are the generation rates for electrons and holes, R_n and R_p are the recombination rates and q is the magnitude of the charge on an electron.

The basic semiconductor equations (1) to (3) are solved self-consistently together with the Helmholtz, lattice heat flow and the photon rate equations. Two-dimensional Helmholtz equation is solved to determine the transverse optical field profile using the effective frequency method (EFM) and it is given by (SILVACO 2007):

$$\nabla^2 E(r,z,\varphi) + \frac{\omega_0^2}{c^2}\varepsilon(r,z,\varphi,\omega)E(r,z,\varphi) = 0 \tag{4}$$

where ω is the frequency, $\varepsilon(r, z, \phi, \omega)$ is the complex dielectric permittivity, $E(r, z, \phi)$ is the optical electric field, and c is the speed of light in vacuum. The photon rate equation is solved in order to obtain the modal photon density, S_m and is given by (SILVACO 2007):

$$\frac{dS_m}{dt} = \left(\frac{c}{N_{eff}}G_m - \frac{1}{\tau_{ph_m}} - \frac{cL}{N_{eff}}\right)S_m + R_{spm} \tag{5}$$

where G_m is the modal gain, R_{spm} is the modal spontaneous emission rate, L represents the losses in the laser, N_{eff} is the group effective refractive index, τ_{ph_m} is the modal photon lifetime and c is the speed of light in vacuum. The heat flow equation has the form (SILVACO 2007):

$$\rho_L C_L \frac{\partial T_L}{\partial t} = \nabla(\kappa \nabla T_L) + H \tag{6}$$

where ρ_L is the material's density, C_L is the specific heat of the crystal lattice, $\varkappa$ is the thermal conductivity, H is the heat power density (W/cm^3) generated by various sources and T_L is the local lattice temperature. This equation relates the change in local temperature to the local heat flux (in or out) and to the local heat generation. Equations (1)-(6) provide an approach that can account for the mutual dependence of electrical, optical and thermal phenomena in the development of a comprehensive VCSEL model. In the active region, the carrier density rate is given by (Wilmsen et al. 1999):

$$\frac{\eta_i dN}{dt} = \frac{1}{qV} - R_{sp} - R_{nr} - gv_g N_p \tag{7}$$

The photon density rate is given by (Wilmsen et al. 1999):

$$\frac{dN_p}{dt} = \Gamma g v_g N_p + \Gamma\beta_{sp} R_{sp} - \frac{N_p}{\tau_p} \tag{8}$$

where η_i is the injection efficiency; I is the terminal current; q is the electronic charge; $V=\pi(DD/2)2L_a$ is the active region volume with device width of DD and thickness L_a; R_{sp} is the spontaneous recombination rate of carriers; R_{nr} is the nonradiative recombination rate; gv_gN_p is the stimulated recombination rate of carriers in which g is the incremental optical gain in the active material and v_g is the group velocity in the axial direction of the mode in question; Γ is the mode confinement factor, β_{sp} is the spontaneous emission factor and τ_p is the photon lifetime in the cavity.

LW-VCSEL MODEL

Figure 1 shows the schematic design of the bottom-emitting, air-post, wafer-bonded, GaAs/InP-based 1.5 μm VCSEL device which was modeled partially-based on the experimental device fabricated in the past (Babic et al. 1997). In this structure, the strained MQW active region consists of six 5.5-nm thick $In_{0.76}Ga_{0.24}As_{0.82}P_{0.18}$ (E_g=0.76 eV) quantum wells and five 8-nm thick $In_{0.48}Ga_{0.52}As_{0.82}P_{0.18}$ barriers. The MQWs are embedded in between InP spacer layers that have been extended by thin GaAs layers on top of each fused mirror to increase emission wavelength. Alternating high- and low-refractive index layers of GaAs (RI=3.38)/$Al_{0.33}Ga_{0.67}As$ (RI=3.05) form the top 30-period p-type DBR whereas the bottom n-type DBR mirror is formed with 28-periods of GaAs/AlAs (RI=2.89) layers.

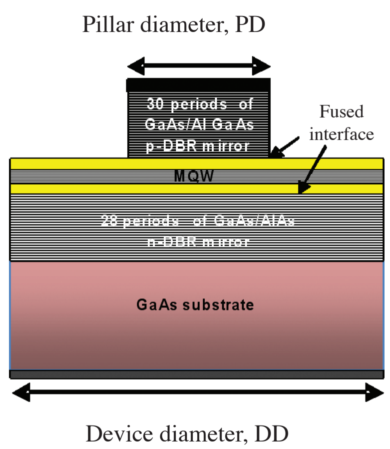

FIGURE 1. Schematic version of LW-VCSEL

Numerical Analysis Results

The LW-VCSEL parameters evaluated in this paper were the device diameter (L_{DD}) and the mesa or pillar diameter (L_{PD}). The device (equivalent to active region diameter as well) was varied from 6 µm until 20 µm while maintaining the mesa diameter at 6 µm and the mesa diameter was varied from 1 µm until 12 µm while maintaining the device diameter at 12 µm. The size of LW-VCSEL devices has a profound effect on its characteristics because as depicted in (7), the larger the volume of the active region, the larger will be the carrier density rate hence producing a device with higher lasing powers. Figures 2 (a) and (b) compare the V-I curve of devices with variation in L_{DD} and L_{PD}. The series resistance R_s reduces from 325 Ω for L_{DD}=8 µm to 287 Ω for L_{DD}=12 µm at a bias voltage of 2 V. The pillar diameter, L_{PD}=4 µm shows a series resistance of 612 Ω and reduces to 95 Ω for devices with L_{PD}=12 µm. At a bias voltage of 2 V, increment in the device and pillar diameter reduces the series resistance since increment in device volume increases the total carrier density rate and subsequently the terminal current. It is observed that variation in the pillar diameter has a more profound impact on the V-I characteristics since it serves as a means for current confinement.

Figures 3 (a) and (b) is a comparison of the L-I curves. Devices with very small mesas or diameter have inadequate carriers and photons hence no/minimum lasing occurs for L_{DD}<10 µm where the emission power is between 4.8 mW to 5.2 mW at a bias voltage of 3 V. Lasing only occurs in devices with L_{PD}>2 µm and the highest lasing power of 6.97 mW was obtained for a device with L_{DD}=12 µm and L_{PD}=12 µm. Figure 4 (a) and (b) compares the lattice temperature effect on the LW-VCSEL with variations in device and pillar/mesa diameter. As with the V-I curves, L_{PD} has a more pronounced effect on the T-I curve since the amount of current injected into the active region is proportional to L_{PD}. At higher currents, the increment in lattice temperature increases with increment in L_{DD}. At an ambient temperature of 300 K, temperature increment was 10°C for L_{DD}=8 µm and 13°C for L_{DD}=18-20 µm. For a larger device volume, more recombination processes

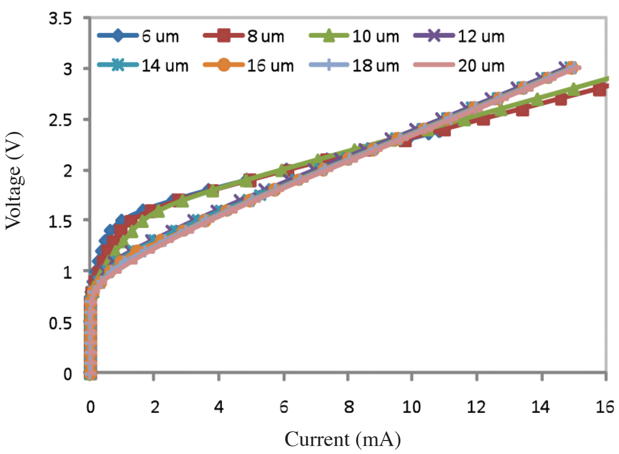

(a)

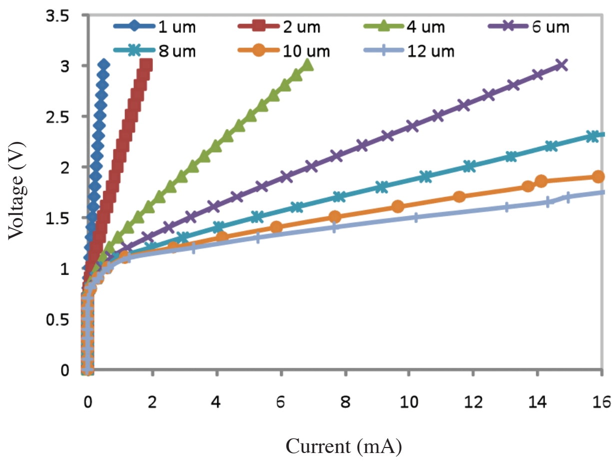

(b)

FIGURE 2. Effects of (a) device diameter and (b) mesa diameter on the V-I curve

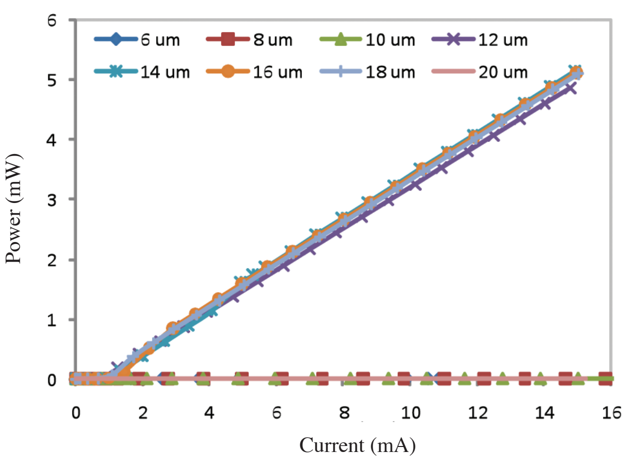

(a)

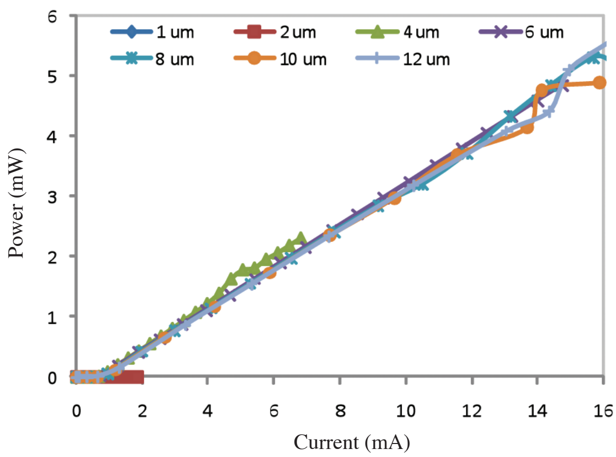

(b)

FIGURE 3. Effects of (a) device diameter and (b) mesa diameter on the L-I curve

results in higher heat generation and increment in lattice temperature. However, increment in L_{PD} shows an opposite trend where increment in the mesa diameter reduces the lattice temperature increment within the device. Lattice temperature was increased by 3°C for L_{PD}=1 μm and 1°C for L_{PD}=12 μm. This could be due to the increment in carrier collisions producing higher heat for a smaller mesa.

Figures 5 (a) and (b) portray the minimal effect of L_{DD} and L_{PD} on the device modal gain where it is maintained at a constant value ~25 cm^{-3} for all lasing devices irrespective of device and mesa diameters. This is because the MQW quantity used in all devices are the same and the same amount of photons contributing to the gain is produced. Figures 6 (a) and (b) gives insight into the peak lasing wavelength, λ_0 of LW-VCSEL with different L_{DD} and L_{PD}. When L_{DD} increases, the peak wavelength is nudged towards longer wavelengths where for L_{DD}= 6 μm, λ_0 is 1.561 μm and for L_{DD}=18 μm, λ_0 is 1.564 μm. This could be due to the increment in the active region length causing the wavelength to increase as well according to the equation $nL=m\lambda/2$ where n is the refractive index, L is the length of the region, m is the propagation mode and λ the wavelength. No effect on λ_0 is observed for variation in L_{PD} because it does not affect the active region. Figures 7 (a) and (b) compares the peak reflectivity of the top and bottom DBR mirrors where for variation in L_{DD}, the top DBR reflectivity is maintained at 99.84% but the reflectivity of the bottom DBR mirror reduces minimally at 99.80% when L_{DD} is increased. Variation in L_{PD} has no effect on the peak reflectivity.

The LW-VCSEL threshold current, I_{th} is compared in Figures 8 (a) and (b) where I_{th} decreases with increment in L_{DD} whereas the opposite effect is observed in increment of L_{PD} where I_{th} increases as well. A larger active region increases photon formation which contributes to a smaller lasing current threshold. On the other hand, a larger mesa diameter reduces the current confinement effect and more leakage current contributes to increment in lasing current threshold. I_{th} is lowest at 0.5 mA for L_{DD}=20 μm and L_{PD}=12 μm.

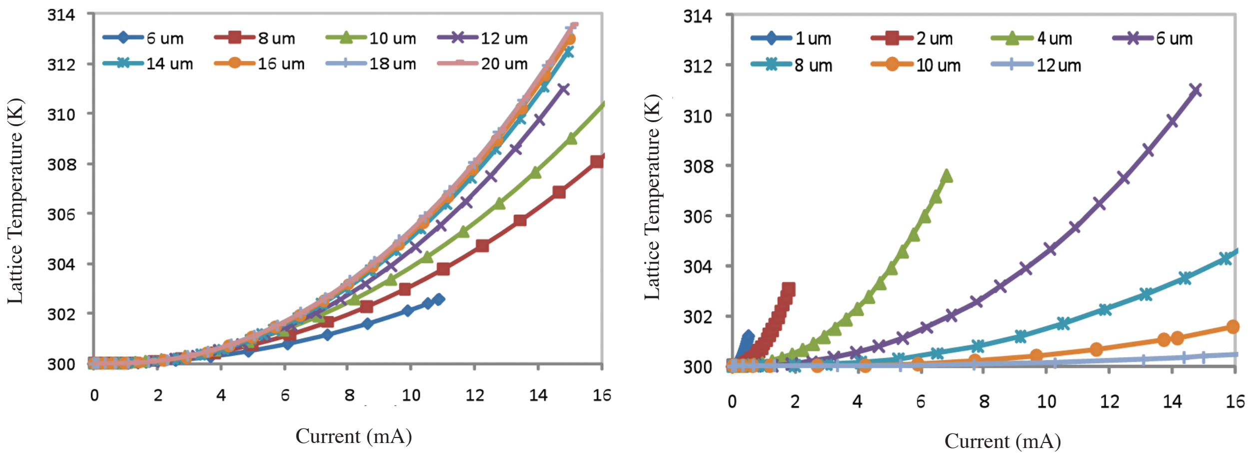

(a) (b)

FIGURE 4. Effects of (a) device diameter and (b) mesa diameter on the Temp-I curve

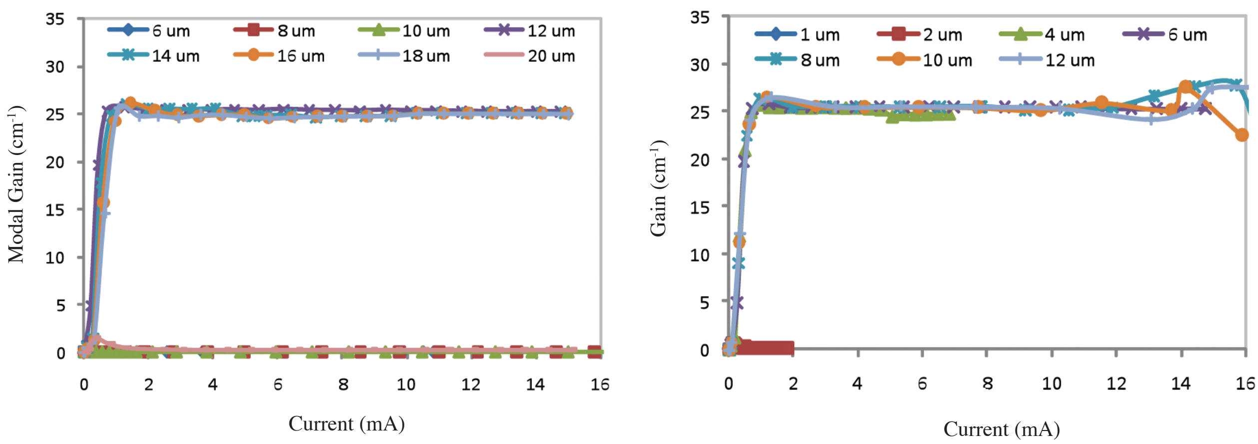

(a) (b)

FIGURE 5. Effects of (a) device diameter and (b) mesa diameter on the modal gain-I curve

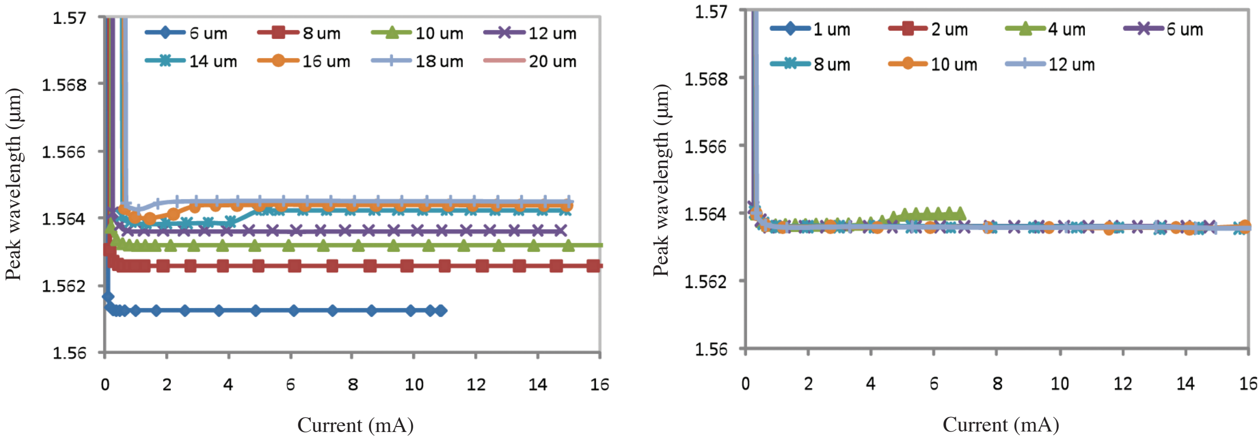

(a) (b)

FIGURE 6. Effects of (a) device diameter and (b) mesa diameter on the modal gain-I curve

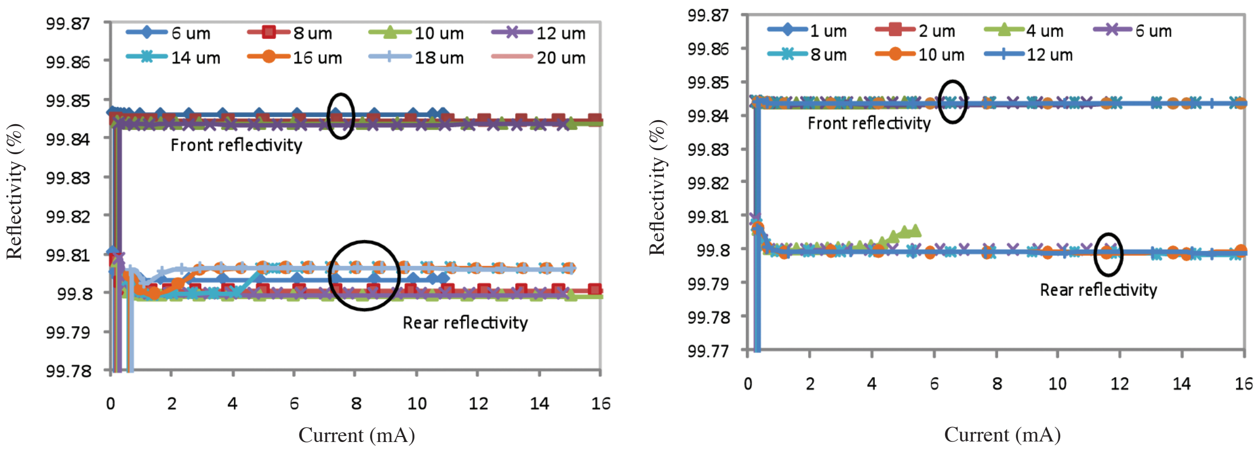

(a) (b)

FIGURE 7. Effects of (a) device diameter and (b) mesa diameter on the reflectivity-I curve

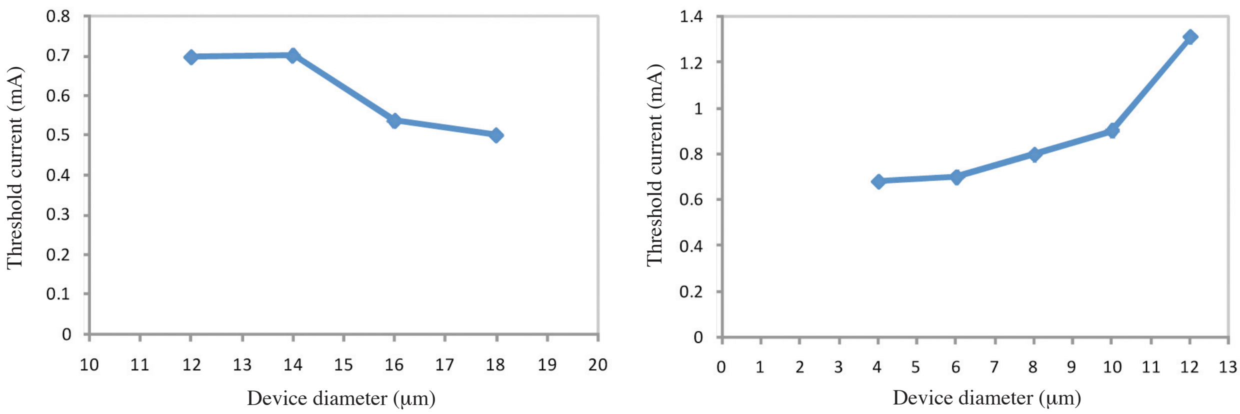

(a) (b)

FIGURE 8. Effects of (a) device diameter and (b) mesa diameter on the threshold current

CONCLUSION

In this paper, we have analyzed the variation effects of both the device and mesa diameter on the characteristics of a double-fused MQW LW-VCSEL. Increment in either the device or pillar diameter, reduces both peak lasing power and nudges the peak wavelength to longer wavelengths.

Devices with large device diameters and small mesa diameters produce lower threshold currents. The best device model produced is for L_{DD}=12 μm and L_{PD}=6 μm with lasing powers of 4.9 mW, lasing wavelength of 1.5 μm and threshold current of ~0.8 mA. The values achieved in the simulated model is comparable if not better compared to the experimental device developed in the past (Babic et al. 1997) where lasing power of 1 mW was achieved at lasing wavelength of 1.55 μm and threshold current of 2.3 mA. The results obtained goes on to proof that numerical simulation provides a suitable platform to evaluate and optimize various device design parameters without increasing fabrication cost and time.

REFERENCES

Babic, D.I., Piprek, J.S., Mirin, K., Margalit, R.P., Mars, N.M., Bowers, D.E. & Hu, J.E. 1997. Design and analysis of double-fused 1.55-μm vertical-cavity lasers. *IEEE Journal of Selected Topics in Quantum Electronics* 33: 1369-1383.

Geske, J., Gan, K.G., Okuno, Y. L., Piprek, J. &. Bowers, J.E. 2004. Vertical-Cavity Surface-Emitting Laser Active Regions for Enhanced Performance With Optical Pumping. *IEEE Journal of Quantum Electronics* 40: 1155-1162.

Hofmann, W. & Amann, M.C. 2008. Long-wavelength vertical-cavity surface-emitting lasers for high-speed applications and gas sensing. *IET Optoelectronics* 2: 134-142.

Kapon, Eli & Sirbu, Alexei. 2009. Power-efficient answer. *Nature Photonics* 3: 27-29.

Karim, A., Piprek, J., Abraham, P., Lofgreen, D., Chiu, Y.J. & Bowers, J.E. 2001. 1.55-μm vertical-cavity laser arrays for wavelength-division multiplexing. *IEEE Journal of Selected Topics in Quantum Electronics* 7: 178-183.

Lin, C.K., Bour, D.P., Zhu, J., Perez, W. H., Leary, M.H., Tandon, A., Corzine, S.W. & Tan, M.R.T. 2003. High temperature continuous-wave operation of 1.3- and 1.55-/spl mu/m VCSELs with InP/air-gap DBRs. *IEEE Journal of Selected Topics in Quantum Electronics* 9: 1415-1421.

Margalit, N.M., Piprek, J., Zhang, S., Babic, D.I., Streubel, K., Mirin, R.P., Wesselmann, J.R. & Bowers. J.E. 1997. 64°C continuous-wave operation of 1.5-μm vertical-cavity laser. *IEEE Journal of Selected Topics in Quantum Electronics* 3: 359-365.

Mehta, M., Feezell, D., Buell, D.A., Jackson, A.W., Coldren, L.A. & Bowers, J.E. 2006. Electrical design optimization of single-mode tunnel-junction-based long-wavelength VCSELs. *IEEE Journal of Selected Topics in Quantum Electronics* 42: 675-682.

Nakagawa, S., Hall, E., Almuneau, G., Kim, J.K., Buell, D.A., Kroemer, H. & Coldren, L.A. 2001. 1.55-μm InP-lattice-matched VCSELs with AlGaAsSb-AlAsSb DBRs. *IEEE Journal on Selected Topics in Quantum Electronics* 7: 224-230.

Nishiyama, N., Caneau, C., Guryanov, G., Liu, X.S., Hu, M. & Zah, C.E. 2003. High efficiency long wavelength VCSEL on InP grown by MOCVD. *Electronics Letters* 39: 437-439.

Ohiso, Y., Okamoto, H., Iga, R., Kishi, K. & Amano, C. 2002. Single transverse mode operation of 1.55-μm buried heterostructure vertical-cavity surface-emitting lasers. *IEEE Photonics Technology Letters* 14: 738-740.

Shau, R., Ortsiefer, M., Rosskopf, J., Bohm, G., Kohler, F. & Amann, M.C. 2001. Vertical-cavity surface-emitting laser diodes at 1.55 μm with large output power and high operation temperature. *Electronics Letters* 37: 1295-1296.

Shin, J.H., Yoo, B.S., Han, W.S., Kwon, O.K., Ju, Y. G. & Lee, J.H. 2002. CW operation and threshold characteristics of all-monolithic InAlGaAs 1.55 μm VCSELs grown by MOCVD. *IEEE Photonics Technology Letters* 14: 1031-1033.

SILVACO International. 2007. *ATLAS User's Manual*, Version 5.12.0.R. USA, SILVACO International Incorporated.

Syrbu, A., Iakovlev, V.P., Berseth, C.A., Dehaese, O., Rudra, A., Kapon, E., Jacquet, J., Boucart, J., Stark, C., Gaborit, F., Sagnes, I., Harmand, J.C. & Raj, R. 1998. 30°C CW operation of 1.52 μm InGaAsP/AlGaAs vertical cavity lasers with in situ built-in lateral current confinement by localised fusion. *Electronics Letters* 34: 1744-1745.

Wilmsen, C., Temkin, H. & Coldren, L.A. 1999. *Vertical-Cavity Surface-Emitting Lasers*, United Kingdom: Cambridge University Press.

Yuen, W., Li, G.S., Nabiev, R.F., Boucart, J., Kner, P., Stone, R.J., Zhang, D., Beaudoin, M., Zheng, T., He, C., Yu, K., Jansen, M., Worland, D.P. & Chang-Hasnain, C.J. 2000. High-performance 1.6 μm single-epitaxy top-emitting VCSEL. *Electronics Letters* 36: 1121-1123.

Institute of Microengineering and Nanoelectronics (IMEN)
Universiti Kebangsaan Malaysia (UKM)
43600 Bangi
Selangor, D.E.
Malaysia

*Corresponding author; email: susi@eng.ukm.my

Received: 25 January 2010
Accepted: 4 March 2010